Journal of Biomedical Optics 5(2), 214–220 (April 2000)

Brain tumor demarcation using optical spectroscopy; an *in vitro* study

Wei-Chiang Lin
Department of Biomedical Engineering
Box 1631, Station B
Vanderbilt University
Nashville, Tennessee 37235

Steven A. Toms
Department of Neurological Surgery
MCN T-4224
Vanderbilt Medical Center
Nashville, Tennesse 37332

Massoud Motamedi
Biomedical Engineering Center
621 Jennie Sealy Hospital, Route 0456
University of Texas Medical Branch
Galveston, TX 77550

E. Duco Jansen
Department of Biomedical Engineering
Box 1631, Station B
Vanderbilt University
Nashville, Tennessee 37235

Anita Mahadevan-Jansen
Department of Biomedical Engineering
Box 1631, Station B
Vanderbilt University
Nashville, Tennessee 37235

Abstract. Optical spectroscopy for brain tumor demarcation was investigated in this study. Fluorescence and diffuse reflectance spectra were measured from normal and tumorous human brain tissues *in vitro*. A fluorescence peak was consistently observed around 460 nm (±10 nm) emission from both normal and tumorous brain tissues using 337 nm excitation. Intensity of this fluorescence peak (F_{460}) from normal brain tissues was greater than that from primary brain tumorous tissues. In addition, diffuse reflectance (Rd) between 650 and 800 nm from white matter was significantly stronger than that from primary and secondary brain tumors. A good separation between gray matter and brain tumors was found using the ratio of F_{460} and Rd at 460 nm (Rd_{460}). Two empirical discrimination algorithms based on F_{460}, Rd_{625}, and F_{460}/Rd_{460} were developed. These algorithms yielded an average sensitivity and specificity of 96% and 93%, respectively.
[S1083-3668(00)00602-X]

Keywords: autofluorescence; diffuse reflectance; brain tumor margin detection; tissue diagnosis.

Paper JBO-42003 received Aug. 23, 1999; revised manuscript received Feb. 4, 2000; accepted for publication Feb. 28, 2000.

1 Introduction

Human brain tumors are typically classified as primary tumors and secondary tumors depending on their origin.[1] Primary tumors originate in the brain and are classified according to the histological basis from which they are derived; for example, gliomas arise from glial tissue. Secondary tumors arise from metastatic primary cancers originating elsewhere in the body. The two chief sources of secondary brain tumors are lung cancer in the male and breast cancer in the female. The normal-tumor boundaries for different primary and secondary brain tumors vary from fingerlike protrusions of tumor cells into normal tissues in glioblastoma multiforme to well-circumscribed nodules with possible surrounding edema in most secondary tumors.[1] It is estimated that approximately 17,000 malignant brain tumors are diagnosed in adults and 1500 in children every year in the United States.[2–4]

The most common initial therapy for primary and secondary brain tumors is surgical resection. Many studies have shown that the degree of resection significantly influences the time to recurrence and the overall survival of brain tumor patients.[5–10] Although primary brain tumors account for only 1.4% of all cancer, the five-year survival rate of these patients (35%) is low.[2] The goal of surgical resection, therefore, is to remove the maximum amount of tumor mass without sacrificing the patient's neurologic function.

Anita Mahadevan-Jansen, Ph.D., Assistant Professor, Department of Biomedical Engineering, Vanderbilt University, Box 1631, Station B, Nashville, Tennessee 37235; E-mail: anitha@vuse.vanderbilt.edu

Currently, surgical navigation systems and ultrasonography are used intraoperatively to help neurosurgeons locate brain tumor and maximize resection. Surgical navigation systems enable neurosurgeons to relate the position of a surgical instrument to structures present in preoperative computerized tomography (CT) or magnetic resonance (MR) images. However, CT or MR imaging may not delineate the exact brain tumor margins. Studies have shown that neoplastic cells can be found in brain tissue outside the apparent tumor margins defined by contrast-enhanced CT or MR imaging.[11,12] More importantly, the accuracy of surgical navigation systems can be degraded by registration error and intraoperative brain deformation which may shift brain tumor margins in image space by more than a centimeter from their actual locations.[13,14] Ultrasonography is able to detect brain tumors because of their hyperechoic characteristics.[15–17] However, peritumoral edema is also hyperechoic, which hampers tumor and tumor margin identification.[15] Thus, despite the applications of these technologies in neurosurgery, significant residual tumor mass is often found to be left behind in patients after craniotomy.[7,18] Neurosurgeons also rely on visual inspection and/or on-site pathology to locate tumors and tumor margins. Visual inspection is subjective and often incorrect as the visual characteristics of many brain tumors mimic that of normal brain. In addition, on-site pathology is expensive and time consuming. Hence, there is a need for an objective, intraoperative real-time system which is capable of accurately differentiating brain tumors from normal brain tissue, thus

Table 1 Histopathological identities of brain tissues used in the *in vitro* study.

Type	Histopathological classification	Number of patients	Number of investigate sites
Normal brain tissue	Gray and white matter	4	49
Primary brain tumors	Astrocytoma	1	7
	Anaplastic astrocytoma	2	12
	Glioblastoma	6	29
	Mixed oligodendroglioma and astrocytoma	3	12
Secondary brain tumors	Metastatic carcinoma	4	18

detecting tumor margins with sub-millimeter spatial resolution.

One potential technique for brain tumor demarcation is optical spectroscopy, such as fluorescence spectroscopy, because it can detect subtle changes in tissue architecture and biochemical composition associated with the progression of disease in near real-time. Optical spectroscopy has been successfully applied to detect disorders of various organ systems (e.g., cervix, skin, etc.) both *in vitro* and *in vivo*.[19–25] Several commercial systems are currently available for clinical diagnosis in the bronchus, cervix, etc. However, relatively few studies have addressed the diagnostic potential of optical spectroscopy in brain tumors.[26,27] Chung et al. reported that fluorescence peaks at 470, 520, and 630 nm emission were measured from human brain tissues *in vitro* at 360, 440, and 490 nm excitation, respectively.[26] Bottiroli et al. observed significant differences in autofluorescence properties between normal and tumorous human brain tissues at 360 nm excitation.[27] The results of these studies were inconclusive in terms of the effectiveness of autofluorescence spectroscopy alone for brain tumor demarcation.

Several investigators have used fluorescence dyes, such as 5-aminolevulinic (ALA), to enhance brain tumor detection.[28–30] Stummer et al. report low sensitivity of this method at margins of infiltrating tumors as the fluorescence dye is not taken up by tumor cells where the blood brain barrier is intact.[30] Moreover, ALA-induced fluorescence spectroscopy encounters additional problems including bleaching of fluorescence due to excessive or prolonged illumination. Consequently, dye-enhanced fluorescence spectroscopy may not be the ideal approach for brain tumor demarcation.

Diffuse reflectance spectroscopy is a fast, noninvasive method used to determine optical properties of a sample. It is typically obtained by illuminating a sample (e.g., tissue) with a broadband white light source.[21,31] Because of the changes in structure and morphology at the cellular and subcellular level, optical properties of human normal brain tissues are very different from that of human brain tumorous tissues.[32,33]

In this study, the potential of using autofluorescence combined with diffuse reflectance was investigated for brain tumor demarcation. Excitation-emission matrices (EEMs) of brain tissues were measured to identify the optimal excitation wavelength(s) for discrimination. Autofluorescence and diffuse reflectance spectra were characterized between normal and various tumorous human brain tissues *in vitro*. Spectral features, such as line shapes and intensity, were analyzed and used to develop optimal discrimination algorithms to differentiate between normal and tumorous (primary and secondary) human brain tissues.

2 Materials and Methods

2.1 Sample Handling

Human brain tissues were obtained from craniotomies and temporal lobectomies performed at Vanderbilt University Medical Center with the approval of the Vanderbilt Institutional Review Board. Brain tissues from twenty patients were obtained for this study and their gross histological identities are listed in Table 1. Following excision, brain tissues were rinsed with isotonic phosphate buffered saline (PBS) to remove residual blood, snap frozen in liquid nitrogen, and then stored at −70 °C. Prior to spectral measurements, brain samples were passively thawed to room temperature and then divided into several sections based on physical appearance. They were kept moist with PBS throughout examinations. Optical spectra were acquired at multiple sites of each brain tissue section [see Table 1]. All brain tissue sections were separately preserved in formalin for pathologic analysis. (History was performed by Dr. Mahlon Johnson, Department of Pathology, Vanderbilt University.)

2.2 Instrumentation

Optical spectra of brain tissues were acquired using two different systems in this study. A standard luminescence spectrometer (LS 50B, Perkin–Elmer Ltd., Beaconsfield, Buckinghamshire, England) was used to measure EEMs of brain samples, which characterize features of fluorescence emission from brain tissues as well as reveal the effective excitation wavelength(s) for brain tissue discrimination following the determination of the optimal excitation wavelength(s). In addition, fluorescence and diffuse reflectance spectra of tissue samples were measured with a system as illustrated in Fig. 1. A high-pressure nitrogen laser (337 nm, Oriel Corporation, Stratford, CT) was used as the excitation source for fluorescence measurements. A 150 W illuminator (Fiber Lite, Model 180, Edmund Scientific Company) emitting broadband white

1083-3668/2000/$15.00 © 2000 SPIE

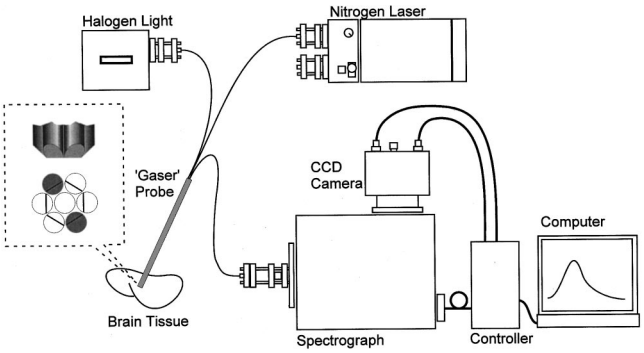

Fig. 1 Schematic of the experimental setup. The insert illustrates the arrangement and modification of optical fibers at the tip of the ''Gaser'' probe.

light from 400 to 850 nm was used for diffuse reflectance measurements. Light delivery and collection were achieved with a ''Gaser'' fiberoptic probe (Visionex, Inc., Atlanta, GA). This probe comprises of seven 300 μm core diameter fibers as shown in Fig. 1. The central fiber is directed conventionally; the tip of the surrounding fibers are tapered to optimize overlap of excitation and collection volumes as shown in the insert in Figure 1.[34] Two of the surrounding fibers deliver laser pulses and white light respectively to the tissue sample while the remaining fibers collect fluorescence emission and diffuse reflectance from the tissue sample sequentially. The collected signal was dispersed with a spectrograph (Triax 180, Instruments S. A., Inc., Edison, NJ) and detected with a thermoelectrically cooled charge-coupled device (CCD) camera (Spectrum One, Instruments S. A., Inc., Edison, NJ). For fluorescence measurements, reflected laser light was eliminated with two 360-nm-long pass filters placed in front of entrance slit of the spectrograph. The entire system was computer controlled.

2.3 Experimental Methods

EEMs were measured from one healthy brain tissue and six tumorous brain tissues at the beginning of this study. Each test sample was placed at the front surface of a triangular quartz cell. The cell was placed in the sample chamber of the spectrometer such that excitation light was illuminated at the sample with a 30° incident angle and emission light was collected from the sample at 60° from the normal. The spot size of the excitation light on the tissue sample was about 1×8 mm. All samples used in this study were large enough to cover the excitation spot. Excitation wavelengths were varied from 250 to 500 nm in 5 nm increments. Correspondingly, the emission wavelengths were varied from 280 to 800 nm in 1 nm increments. The spectral resolution was 5 nm for the excitation and 7 nm for the emission monochromator. The scanning speed was set at 750 nm/min. The time required for each EEM was 20 min. All EEM measurements were corrected for wavelength dependence of illumination intensity and nonuniform spectral response all components in the spectrometer.

Following the EEM study, fluorescence and diffuse reflectance spectra were measured from brain tissue samples with the spectroscopic system shown in Figure 1. The fiberoptic probe was placed directly in contact with the tissue sample during each measurement. The output power of white light source was maintained at 30 mW. The nitrogen laser was operated at 20 Hz repetition rate, 5 ns pulse width, and average pulse energy of 6.5 μJ. An integration time of 2 s was used in all measurements to achieve high signal-to-noise ratio. Three spectra were acquired at each investigated site of brain samples: the baseline $B(\lambda)$ (i.e., measured with no excitation light), the fluorescence spectrum $F(\lambda)$, and the reflectance spectrum $Rd(\lambda)$. Spectra from a fluorescence and reflectance standard [i.e., $F_{\mathrm{ref}}(\lambda)$ and $Rd_{\mathrm{ref}}(\lambda)$] were measured at the end of each experiment to monitor changes in laser pulse energy, white light power, and other instrumental parameters. The fluorescence standard consists of a dilute concentration of Rhodamine 6G solution (2 mg/L) in ethylene glycol contained in a quartz cuvette. The reflectance standard was a 20% reflectance plate (Labsphere, North Sutton, NH) placed in a sealed black box.

2.4 Data Analysis

Spectral data were post-processed before any analysis was conducted. Background subtraction was first performed on each spectrum with its corresponding baseline measurement. Correction factors (C) were generated by taking ratios between the standard spectra [$S(\lambda)$] measured at the start of the study and those acquired for every experiment of the study.

$$C_i = S_i(\lambda)/S_1(\lambda), \tag{1}$$

where $S(\lambda)=F_{\mathrm{ref}}(\lambda)$ or $Rd_{\mathrm{ref}}(\lambda)$, $\lambda=620$ nm for fluorescence, 700 nm for reflectance, $i=1$ to n, n is the total number of experiments. Each correction factor C_i was then multiplied to every sample spectrum acquired in a given experiment i, thus ensuring spectral intensity as valid discrimination information.

All fluorescence spectra were corrected for the nonuniform spectral response of the detection system using correction factors obtained by recording the spectrum of an National Institute of Standards and Technology (NIST) traceable calibration tungsten ribbon filament lamp. Reflectance spectra were multiplied by wavelength-dependent factors to account for nonuniform spectral response of the detection system as well as spectral emission of the reflectance light source. These factors were derived from the reflectance measurement of a mirror with a known wavelength-dependent reflectivity (10R08ER.1, Newport Corporation, Irvine, CA). After post-processing, changes in fluorescence and reflectance spectra, such as intensity and line shape, were correlated with histopathological identities of brain tissue sections. Empirical diagnostic algorithms were developed based on intensity, line shape, and ratio of fluorescence and diffuse reflectance spectra for separating tumorous brain tissues from normal brain tissues.

3 Results

Figure 2 is an example of an EEM measured from a human brain sample (i.e., cortex). EEMs of normal and malignant brain tissues show only two distinct fluorescence peaks; one at 290 nm excitation, 350 nm (±5 nm) emission, and another at 330 nm excitation, 460 nm (±10 nm) emission. Both fluorescence peaks were compared among the brain tissue samples. The intensity of the fluorescence peak at 330 nm excitation, 460 nm emission was found to be consistently

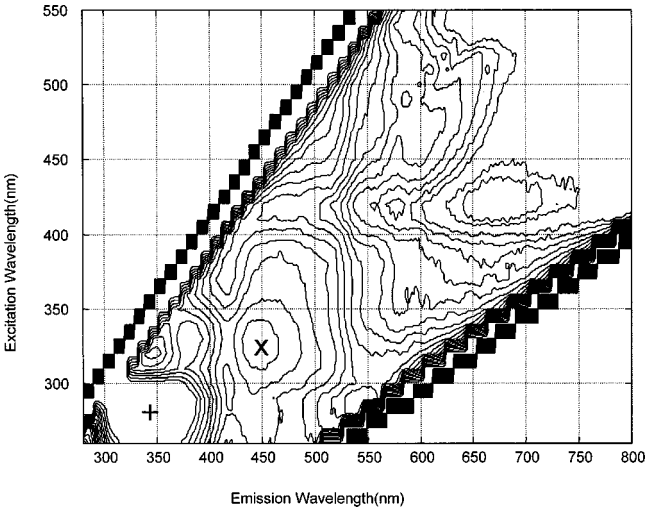

Fig. 2 Excitation-emission matrix of normal human cortex. Two pronounced fluorescence peaks are shown in this EEM; one at 290 nm excitation, 350 nm emission (+), and another at 330 nm excitation, 450 nm emission (×).

lower in brain tumorous tissues than that in normal brain tissues. In addition, a small shift in peak location of this fluorescence emission was observed in brain tumors compared to normal brain tissues. These observations suggested that the fluorescence peak at 330 nm excitation, 460 nm emission would maximize the capability of brain tissue discrimination based on fluorescence. Therefore, 337 nm (i.e., nitrogen laser, closest to 330 nm) was selected as the optimal excitation wavelength for further study.

Fluorescence and diffuse reflectance spectra from 127 investigated sites in brain samples from 20 patients, including those used in the EEM study, were measured using the system described in Figure 1. Figure 3 shows the representative fluorescence [Figure 3(a)] and diffuse reflectance [Figure 3(b)] spectra acquired from normal human brain tissues and different types of human brain tumors. In general, the fluorescence intensity at 460 nm emission of normal gray and white matter was found to be greater than that of primary and secondary tumor tissues. This observation was consistent with that made from EEM measurements. Diffuse reflectance of most brain tissues reached the maximum around 625 nm and then decreased gradually as wavelength increased. Above 600 nm where blood absorption has the least influence, diffuse reflectance of white matter was much more intense than that of other brain tissues. However, diffuse reflectance of gray matter was similar to that of tumor tissues above 600 nm. Valleys at 415, 542, and 577 nm due to hemoglobin/oxyhemoglobin (Hb/HbO_2) absorption were clearly seen in fluorescence as well as diffuse reflectance spectra of brain tissues. No consistent differences, however, could be observed in the line shape of fluorescence and diffuse reflectance spectra between normal and malignant brain tissues.

All fluorescence and diffuse reflectance spectra were processed using the methods described in Sec. 2. Processed spectra from all brain tissues were analyzed in terms of intensities and ratios of intensities at different wavelengths to identify parameters that separate different brain tissue types. In addition, fluorescence spectra of all samples were normalized to

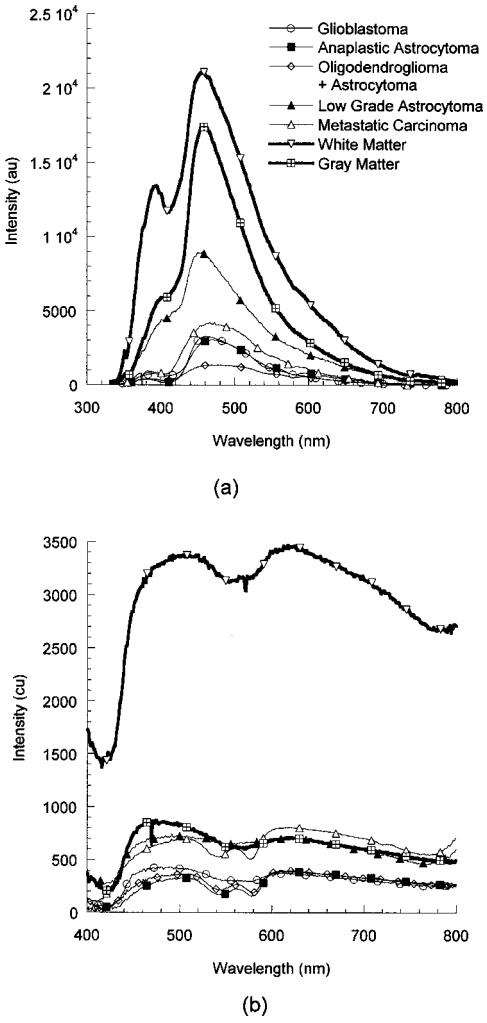

Fig. 3 Typical *in vitro* (a) fluorescence and (b) diffuse reflectance spectra of different types of brain tissues.

their maximum to study the changes in line shape. Results of the analysis suggest different algorithms are required for separation of primary brain tumors and normal brain tissues as compared to secondary brain tumors and normal brain tissues.

Figure 4(a) shows the fluorescence intensity at 460 nm emission (F_{460}) plotted with respect to the diffuse reflectance intensity at 625 nm (Rd_{625}) for all normal tissues and primary tumor tissues. A clear separation between normal brain tissues and primary brain tumors was observed along the F_{460} axis but not along the Rd_{625} axis. The figure indicates that fluorescence alone can differentiate normal brain tissues from primary brain tumors. Although reflectance spectra can be used to separate the samples based on white matter content, reflectance alone cannot separate between normal and tumor tissues. A simple one-dimensional discrimination algorithm, using a F_{460} of 10 000 calibrated units (c.u.) as the cutoff, yields a sensitivity and specificity of 97% and 96%, respectively, in separating primary brain tumors from normal brain tissues. Only two investigated sites in brain tumor samples and one in healthy gray matter were misclassified [see Figure 4(a)]. The same discrimination algorithm was also applied to the secondary brain tumors, which is shown in Figure 4(b). However,

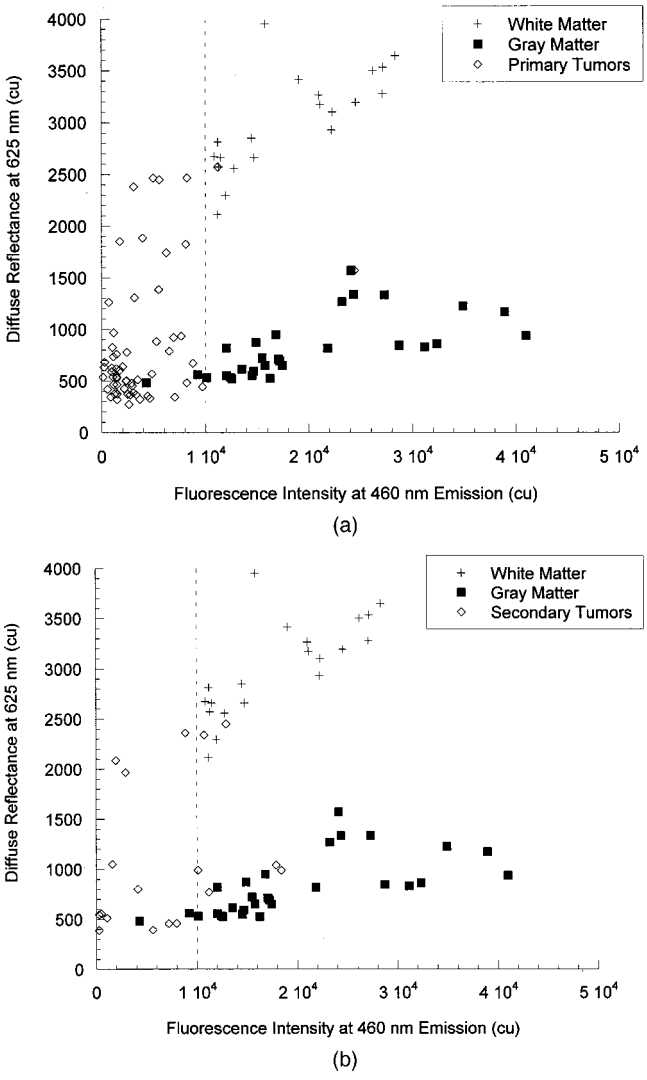

Fig. 4 A scatter plot of F_{460} vs Rd_{625} of (a) normal brain tissues and primary brain tumors, and (b) normal brain tissues and secondary brain tumors. The dashed line represents the cutoff (F_{460}=10 000 c.u.) used for the one-dimensional discrimination algorithm based on fluorescence spectroscopy alone.

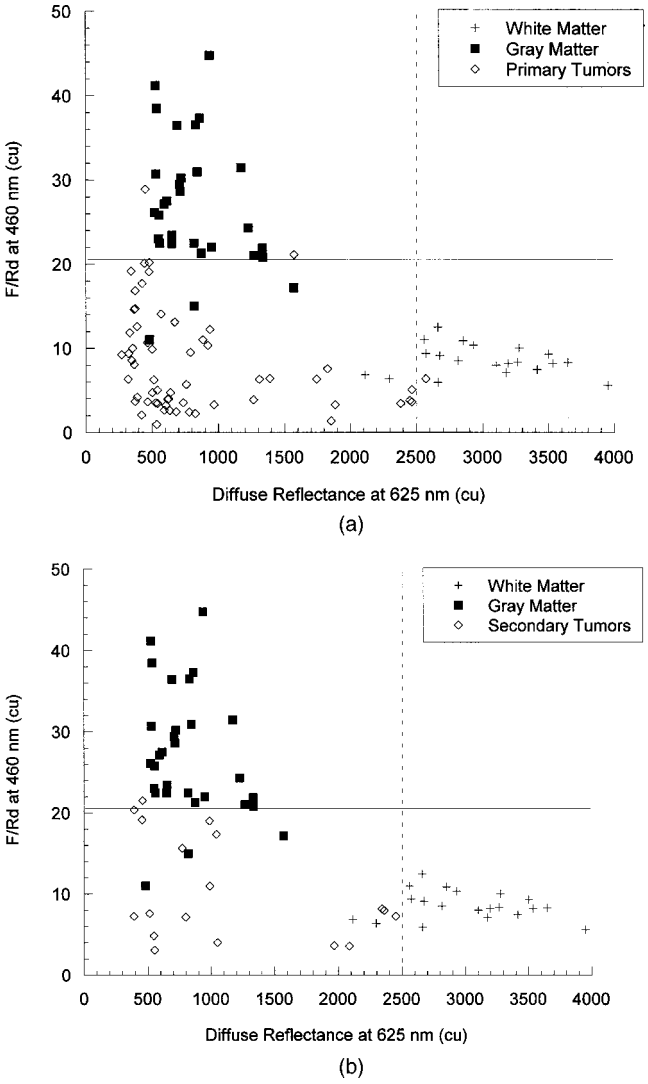

Fig. 5 A scatter plot of F_{460}/Rd_{460} vs Rd_{625} of (a) normal brain tissues and primary brain tumors, and (b) normal brain tissues and secondary brain tumors. The dashed line (Rd_{625}=2500 c.u.) and the solid line (F_{460}/Rd_{460}=20.5) are used together for the two-dimensional discrimination algorithm based on combined fluorescence and diffuse reflectance spectroscopy.

this algorithm only yielded a sensitivity of 67% in separating secondary brain tumors from normal brain tissues (Table 2).

A different empirical discrimination algorithm was developed for discriminating secondary brain tumors from normal brain tissues using the ratio of fluorescence emission and diffuse reflectance at 460 nm (F_{460}/Rd_{460}) and Rd_{625}. Figure 5(b) shows a scatter plot of F_{460}/Rd_{460} with respect to Rd_{625} for all normal brain tissue samples and secondary brain tumors. Using F_{460}/Rd_{460} of 20.5 and Rd_{625} of 2500 as cutoffs, this algorithm yields a sensitivity of 94% and specificity of 90% for differentiating secondary brain tumors from normal brain tissues. Only one secondary brain tumor sample was misclassified as a normal brain tissue. The same discrimination algorithm was also applied to primary brain tumors [see Figure 5(a)], which yields a sensitivity of 95% and specificity of 90%. Thus, the sensitivity and specificity of this algorithm for separating all brain tumors and normal brain tissues are 96% and 90%, respectively.

4 Discussion and Conclusions

The goal of this *in vitro* study was to assess the potential of optical spectroscopy for brain tumor detection. Spectra ac-

Table 2 Sensitivity and specificity of the two spectroscopic diagnostic algorithms.

	Primary		Secondary	
Algorithm	Sensitivity, %	Specificity, %	Sensitivity, %	Specificity, %
F_{460}	97	96	67	96
F_{460}/Rd_{460} and Rd_{625}	95	90	94	90

quired from 127 investigated sites in brain sections from 20 patients show that empirical discrimination algorithms with a high specificity and sensitivity can be easily developed using fluorescence at 460 nm emission and diffuse reflectance at 460 and 625 nm. These results attest the validity of using combined fluorescence and diffuse reflectance spectroscopy for discrimination of primary and secondary tumors from normal brain tissues. This is the first essential step towards the development of the technique for brain tumor demarcation.

All fluorescence spectra acquired in this study exhibit only one fluorescence peak at 460 nm (± 10 nm) emission using 337 nm excitation or longer. This observation is different from that reported previously by Chung et al.[26] in which multiple fluorescence peaks were measured at various excitation wavelengths. In addition, no definite change in the line shape is found between the fluorescence spectra of normal brain tissues and those of brain tumors. The fluorescence based empirical discrimination developed in this study, therefore, only utilizes the fluorescence intensity of 460 nm emission (F_{460}) [see Figure 4]. This discrimination algorithm performs very well in separating primary brain tumors from normal brain tissues; sensitivity of 97% and specificity of 96% are achieved. The success of this algorithm is attributed to F_{460} which is consistently lower in primary brain tumors than that in normal brain tissues. However, this fluorescence based discrimination algorithm is less effective in separating secondary brain tumors from normal brain tissues due to strong F_{460} from some secondary brain tumors [see Figure 4(b)].

To circumvent the limitation of the fluorescence based algorithm in differentiating secondary brain tumors, a second discrimination algorithm was developed based on combined fluorescence and diffuse reflectance, F_{460}/Rd_{460} and Rd_{625} [see Figure 5]. The ratio of F_{460} and Rd_{460} is used to reduce fluorescence spectral distortion introduced by tissue reabsorption and scattering.[35–38] Rd_{625} is selected because of the differences in its intensity between different brain tissue types with minimum influence from absorption of Hb/HbO_2. This algorithm is effective in differentiating secondary brain tumors from normal brain tissues, with a sensitivity of 94% and specificity of 90%. It separates all brain tumors from normal brain tissue with a sensitivity and specificity of 96% and 90%. It should be noted that both algorithms were developed based on the current data set and should be considered as biased.

Tissue fluorescence intensity is determined not only by the concentration of natural fluorophores within the tissue but also by the optical properties of the tissue. Hence, interpreting changes in the fluorescence spectra of various brain tissue types is complex. It has been suggested that the concentration of many natural fluorophores, such as nicotinamide adenine dinucleotide (NADH), varies between normal and malignant tissues. In addition, increase in hemoglobin content, which leads to an increase in absorption coefficient at 337 nm as well as 460 nm, could also reduce the fluorescence intensity at 460 nm emission. However, the specific cause(s) for the variations in the fluorescence intensity at 460 nm emission in the different brain tissues types has yet to be uncovered and needs to be studied. Nevertheless, the interdependence of tissue optics and the fluorescence emission indicates that the accuracy of a discrimination algorithm based on fluorescence intensity alone may be degraded by, for example, blood contamination.

Distinct architectural changes at the cellular and subcellular level are exhibited between normal and malignant brain tissues. For example, brain white matter is relatively anuclear but most aggressive tumors are characterized with a high density of cells (and therefore nuclei) and a higher nuclear-cytoplasmic ratio.[39,40] Thus optical properties vary significantly between different brain tissue types.[32,33] However, diffuse reflectance alone is insufficient for brain tissue discrimination as the level of diffuse reflectance from gray matter is very similar to those from brain tumors as shown in Figures 4(a) and 4(b). This may seem incoherent with the optical properties measurements of brain tissues reported by Eggert and Blazek; who found that the ratio of absorption and scattering coefficient from gray matter is lower than that from brain tumors, especially between 600 and 800 nm.[32] However, it should be noted that the intensity of diffuse reflectance at a fixed radial position $[Rd(r)]$ does not necessarily correlate linearly to the variations in absorption and scattering coefficients of tissue samples. Hence the same $Rd(r)$ may be measured from two samples with different optical properties. This has been verified with a Monte Carlo simulation program [unpublished data].

The *in vitro* study presented in this paper shows the potential of using optical spectroscopy to differentiate brain tumor from normal brain tissues. However, the spectral characteristics of brain tumor margins, especially of infiltrating type, with respect to normal and tumorous brain tissues needs to be studied *in vivo* and it was not possible to obtain *in vitro* brain tumor margin samples. In order to truly evaluate the clinical merit of this combined spectroscopic technique for brain tumor and tumor margin detection, human clinical trials are currently in progress. The result of this clinical trial will be reported in the future.

Acknowledgments

The authors wish to thank Dr. Mahlon Johnson, Chad Lieber, and Glen Henbest for their support and help. The authors acknowledge the financial support of the Laser Fellowship Program from the W. M. Keck Foundation FEL Center, Vanderbilt University, and the Whitaker Special Opportunity Award.

References

1. J. Poirier, F. Gray, and R. Escourolle, in *Manual of Basic Neuropathology*, pp. 17–56, W. B. Saunders Company, Philadelphia (1990).
2. ACS, ''Brain and Spinal Cord Cancers of Adults,'' American Cancer Society, Web Page (1998).
3. M. Chamberlain and P. Kormanik, ''Practical guidelines for the treatment of malignant gliomas,'' *West. J. Med.* **168**, 114–120 (1998).
4. P. Duffner, M. Horowitz, J. Krischer, H. Friedman, P. Burger, and M. Cohen, ''Postoperative chemotherapy and delayed radiation in children less than three years of age with malignant brain tumors,'' *N. Engl. J. Med.* **328**, 1725–1731 (1993).
5. D. Mohan, J. Suh, J. Phan, P. Kupelian, B. Cohen, and G. Barnett, ''Outcome in elderly patients undergoing definitive surgery and radiation therapy for supratentorial glioblastoma multiforme at a tertiary care institution,'' *Int. J. Radiat. Oncol., Biol., Phys.* **42**, 981–987 (1998).
6. M. Selch, B. Goy, S. Lee, S. El-Sadin, P. Kincaid, S. Park, and H. Withers, ''Gangliogliomas: experience with 34 patients and review of the literature,'' *Am. J. Clin. Oncol.* **21**, 557–564 (1998).
7. M. Ammirati, N. Vick, and Y. Liao, ''Effect of the extent of surgical resection on survival and quality of life in patients with supratentorial

glioblastoma and anaplastic astrocytoma,'' *Neurosurgery* **21**, 201–206 (1987).
8. I. Ciric, M. Ammirati, N. Vick, and M. Mikhael, ''Supratentorial gliomas: Surgical considerations and immediate postoperative results: Gross total resection versus partial resection,'' *Neurosurgery* **21**, 21–26 (1987).
9. M. Salcman, H. Scholtz, R. Kaplan, and S. Kulik, ''Long-term survival in patients with malignant astrocytoma,'' *Neurosurgery* **34**, 213–219 (1994).
10. C. Vecht, C. Avezaat, W. van Putten, W. Eijkenboom, and S. Stefanko, ''The influence of the extent of surgery on the neurologic function and survival in malignant glioma. A retrospective analysis in 243 patients,'' *J. Neurol. Neurosurg. Psych.* **53**, 466–471 (1990).
11. G. M. Greene, P. W. Hitchon, R. L. Schelper, W. Yuh, and G. N. Dyste, ''Diagnostic yield in CT-guided stereotactic biopsy of glioma,'' *J. Neurosurg.* **71**, 494–497 (1989).
12. P. LeRoux, T. Winter, M. Berger, L. Mack, K. Wang, and J. Elliott, ''A comparison between preoperative magnetic resonance and intraoperative ultrasound tumor volumes and margins,'' *J. Clin. Ultrasound* **22**, 29–36 (1994).
13. D. Hill, C. J. Maurer, R. Maciunas, J. Barwise, J. Fitzpatrick, and M. Wang, ''Measurement of intraoperative brain surface deformation under a craniotomy,'' *Neurosurgery* **43**, 514–526 (1998).
14. N. Dorward, O. Alberti, B. Velani, F. Gerritsen, W. Harkness, N. Kitchen, and D. Thomas, ''Postimaging brain distortion: magnitude, correlates, and impact on neuronavigation,'' *J. Neurosurg.* **88**, 656–662 (1998).
15. L. M. Auer and V. V. Velthoven, *Intraoperative Ultrasound Imaging in Neurosurgery: Comparison with CT and MRI*, Springer-Verlag, Berlin (1990).
16. J. E. Knake, R. A. Bowerman, T. M. Silver, and S. McCracken, ''Neurosurgical applications of intraoperative ultrasound,'' *Radiological Clinics of North America* **23**, 73–90 (1985).
17. C. Giorgi and D. Casolino, ''Preliminary clinical experience with intraoperative stereotactic ultrasound imaging,'' *Stereotact Funct Neurosurg.* **68**, 54–58 (1997).
18. A. Kowalczuk, R. L. Macdonald, C. Amidei, G. Dohrmann, R. K. Erickson, J. Hekmatpanah, S. Krause, S. Krishnasamy, G. Masters, S. F. Mullan, A. J. Mundt, P. Sweeney, E. E. Vokes, B. K. Weir, and R. L. Wollman, ''Quantitative imaging study of extent of surgical resection and prognosis of malignant astrocytomas,'' *Neurosurgery* **41**, 1028–1038 (1997).
19. E. S. Andersson, J. Johansson, K. Svanberg, and S. Svanberg, ''Fluorescence imaging and point measurements of tissue: applications to the demarcation of malignant tumors and atherosclerotic lesions from normal tissue,'' *Photochem. Photobiol.* **53**, 807–814 (1991).
20. A. Gillenwater, R. Jacob, R. Ganeshappa, B. Kemp, A. El-Naggar, J. Palmer, G. Clayman, M. Mitchell, and R. Richards-Kortum, ''Noninvasive diagnosis of oral neoplasia based on fluorescence spectroscopy and native tissue autofluorescence,'' *Arch. Otolaryngol. Head Neck Surg.* **124**, 1251–1258 (1998).
21. I. J. Bigio and J. R. Mourant, ''Ultraviolet and visible spectroscopies for tissue diagnostics: fluorescence spectroscopy and elastic-scattering spectroscopy,'' *Phys. Med. Biol.* **42**, 803–814 (1996).
22. A. H. Ding, ''N2 laser in diagnosis of early cervical cancer,'' *Chung Hua Fu Chan Ko Tsa Chih* **26**, 95–96 (1991).
23. J. Hung, S. Lam, J. C. LeRiche, and B. Palcic, ''Autofluorescence of normal and malignant bronchial tissue,'' *Lasers Surg. Med.* **11**, 99–105 (1991).
24. M. F. Mitchell, S. B. Cantor, N. Ramanujam, G. Tortolero-Luna, and R. Richards-Kortum, ''Fluorescence spectroscopy for diagnosis of squamous intraepithelial lesions of the cervix,'' *Obstet. Gynecol. (N.Y.)* **93**, 462–470 (1999).
25. N. Ramanujam, M. F. Mitchell, A. Mahadevan, S. Thomsen, A. Malpica, T. Wright, N. Atkinson, and R. Richards-Kortum, ''Spectroscopic diagnosis of cervical intraepithelial neoplasia (CIN) in vivo using laser-induced fluorescence spectra at multiple excitation wavelengths,'' *Lasers Surg. Med.* **19**, 63–74 (1996).
26. Y. G. Chung, J. A. Schwartz, C. M. Gardner, R. E. Sawaya, and S. L. Jacques, ''Diagnostic potential of laser-induced autofluorescence emission in brain tissue,'' *J. Korean Med. Sci.* **12**, 135–142 (1997).
27. G. Bottiroli, C. AC, D. Locatelli, R. Nano, E. Giombelli, A. Messina, and E. Benericetti, ''Brain tissue autofluorescence: an aid for intraoperative delineation of tumor resection margins,'' *Cancer Detect Prev.* **22**, 330–339 (1998).
28. T. J. MacDonald, P. Tabrizi, H. Shimada, B. V. Zlokovic, and W. E. Laug, ''Detection of brain tumor invasion and micrometastasis in vivo by expression of enhanced green fluorescent protein,'' *Neurosurgery* **43**, 1437–1442; discussion 1442–1443 (1998).
29. W. S. Poon, K. T. Schomacker, T. F. Deutsch, and R. L. Martuza, ''Laser-induced fluorescence: experimental intraoperative delineation of tumor resection margins,'' *J. Neurosurg.* **76**, 679–686 (1992).
30. W. Stummer, S. Stocker, S. Wagner, H. Stepp, C. Fritsch, C. Goetz, A. E. Goetz, R. Kiefmann, and H. J. Reulen, ''Intraoperative detection of malignant gliomas by 5-aminolevulinic acid-induced porphyrin fluorescence,'' *Neurosurgery* **42**, 518–525; discussion 525–526 (1998).
31. A. Bono, S. Tomatis, C. Bartoli, G. Tragni, G. Radaelli, A. Maurichi, and R. Marchesini, ''The ABCD system of melanoma detection: a spectrophotometric analysis of the asymmetry, border, color, and dimension,'' *Cancer (N.Y.)* **85**, 72–77 (1999).
32. H. R. Eggert and V. Blazek, ''Optical properties of normal human intracranial tissues in the spectral range of 400 to 2500 nm,'' *Adv. Exp. Med. Biol.* **333**, 47–55 (1993).
33. L. O. Svaasand and R. Ellingsen, ''Optical properties of human brain,'' *Photochem. Photobiol.* **38**, 293–299 (1983).
34. ''Gaser Light Management System,'' http://www.visionex-inc.com/gaser.html.
35. R. Alfano and N. Zhadin, ''Correction of the internal absorption effect in fluorescence emission and excitation spectra from absorbing and highly scattering media; theory and experiment,'' *J. Biomed. Opt.* **3**, 171–186 (1998).
36. C. Gardner, S. Jacques, and A. Welch, ''Fluorescence spectroscopy of tissue: recovery of intrinsic fluorescence from measured fluorescence,'' *Appl. Opt.* **35**, 1780–1792 (1996).
37. J. Wu, M. Feld, and R. Rava, ''Analytical model for extracting intrinsic fluorescence in turbid media,'' *Appl. Opt.* **32**, 3585–3595 (1993).
38. H. Zeng, C. MacAulay, D. McLean, and B. Palcic, ''Spectroscopic and microscopic characteristics of human skin autofluorescence emission,'' *Photochem. Photobiol.* **61**, 639–645 (1995).
39. J. Nelson, J. Parisi, and S. Schochet, Jr., *Principles and Practice of Neuropathology*, Mosby, St. Louis (1993).
40. A. Burt, *Textbook of Neuroanatomy*, W. B. Saunders Company, Philadelphia (1993).